Research Article Vol. 5, No. 4 / April 2018 / Optica 434

Relativistic few-cycle pulses with high contrast from picosecond-pumped OPCPA

Alexander Kessel,[1] Vyacheslav E. Leshchenko,[1,*] Olga Jahn,[1] Mathias Krüger,[1] Andreas Münzer,[1] Alexander Schwarz,[1] Vladimir Pervak,[1,2] Michael Trubetskov,[1] Sergei A. Trushin,[1] Ferenc Krausz,[1,2] Zsuzsanna Major,[1,2] and Stefan Karsch[1,2]

[1]Max-Planck-Institut für Quantenoptik, Hans-Kopfermann-Str. 1, 85748 Garching, Germany
[2]Department für Physik, Ludwig-Maximilians-Universität München, Am Coulombwall 1, 85748 Garching, Germany
*Corresponding author: vyacheslav.leshchenko@mpq.mpg.de

Received 2 November 2017; revised 14 February 2018; accepted 20 February 2018 (Doc. ID 308448); published 9 April 2018

For experiments in plasma, nuclear, and high-energy physics, there is a strong demand for laser pulses exhibiting relativistic intensity, few-cycle pulse duration, and a very high contrast. Here we present a picosecond-pumped optical parametric chirped pulse amplification (OPCPA) system delivering pulses at 10 Hz repetition rate with the following key parameters: a compressed pulse duration of less than 7 fs (close to the Fourier limit), a contrast of better than 10^{11} starting from 1 ps before the main pulse, and a peak intensity of 6.9×10^{19} W/cm^2 achieved with an off-axis parabolic mirror (f/1.6). In a proof-of-principle experiment, these pulses were used to generate high harmonics from solid surfaces with photon energies exceeding 55 eV. These results underline the promising perspectives of the reported system for relativistic light–matter interaction experiments and attosecond science. © 2018 Optical Society of America under the terms of the OSA Open Access Publishing Agreement

OCIS codes: (190.4970) Parametric oscillators and amplifiers; (140.7090) Ultrafast lasers; (190.7110) Ultrafast nonlinear optics; (190.4360) Nonlinear optics, devices.

https://doi.org/10.1364/OPTICA.5.000434

1. INTRODUCTION

Advances in the development of high-intensity light sources over the last decades have opened the opportunity for the experimental study of phenomena in plasma, nuclear, and high-energy physics [1]. For many relativistic light–matter interactions such as the generation of intense isolated attosecond pulses from solid surfaces [2], there are three key requirements for the driving pulses: a few-cycle pulse duration, relativistic peak intensities, and an ultrahigh temporal contrast. More specifically, in the context of this paper a pulse is termed "few-cycle" if its electric field comprises less than three oscillations, which allows the detection of field-dependent effects via the carrier-envelope phase (CEP) if it is controlled or at least measured ("tagged") [3,4]. The relativistic regime is accessed at intensities higher than 1.37×10^{18} W $\cdot$ cm$^{-2}/\lambda_c^2$[μm] corresponding to the situation that the quiver energy of an electron placed in the electric field of an optical pulse with central wavelength of λ_c exceeds the electron rest energy. At such intensities a high temporal contrast is vital to avoid detrimental plasma formation before the interaction with the main pulse. In practice this means that the pre-pulse background may not be higher than 10^9–10^{12} W/cm^2 (depending on the temporal structure of the pre-pulse features and the material of the target [5]), which requires a contrast ratio of more than ten orders of magnitude. For light pulses with higher peak intensities, the contrast requirements become correspondingly even more demanding.

Most of the existing systems fulfill just one or two of the three requirements mentioned above: relativistic intensity at multi-terawatt (TW) to petawatt (PW) peak power has been demonstrated by laser systems based on chirped pulse amplification (CPA) [6,7], optical parametric CPA (OPCPA) [8,9,10], and hybrid amplification [11,12], but the listed systems are limited to multi-cycle pulse durations of 15–25 fs and generally face problems with the temporal contrast. Light sources with few-cycle pulse duration, on the other hand, typically do not (or just about) reach the relativistic regime [13,14]. To our knowledge, there are currently only two OPCPA systems that are close to the discussed goal: the LWS20 (4.5 fs, 18 TW, 10 Hz) [15] and a system designed for the Extreme Light Infrastructure–Attosecond Light Pulse Source (ELI-ALPS) project (8 fs, 5.5 TW, 1 kHz) [16]. However, both systems exhibit a poor contrast in the time window of about ±20 ps around the main pulse. This limitation originates from parametric superfluorescence generated within the relatively long pump pulse duration of ~100 ps and can pose problems for some applications.

There are various approaches to improve the temporal contrast of high-intensity laser pulses after amplification, but these approaches increase the complexity of the respective systems and lead to additional drawbacks and limitations. For instance, a contrast improvement of 2–4 orders of magnitude can be achieved using a plasma mirror [5]—typically a glass substrate that reflects

Corrected 17 April 2018

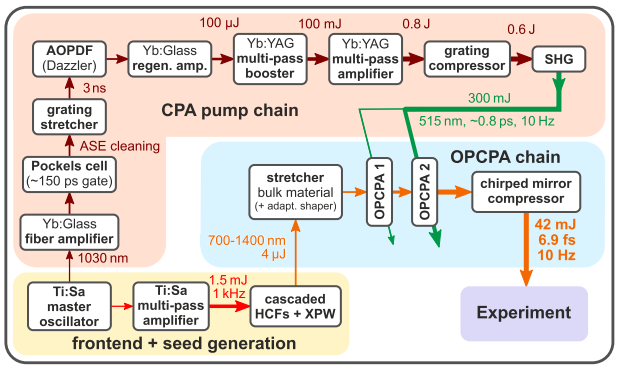

Fig. 1. Conceptual scheme of the petawatt field synthesizer.

the focused beam. This technique, however, results in energy losses of 20–50% [5,17]. Additionally, as the reflected light pulses locally destroy the surface of the plasma mirror, a fresh spot has to be provided after each shot requiring a movable mirror holder and limiting the total number of shots. Moreover, the contrast of the input pulses already has to be sufficiently high to prevent the generation of a pre-plasma that would otherwise severely impair the performance of the technique.

An interesting idea to address the problem of long pulse durations provided by classical laser systems is published in [18]: it is based on nonlinear compression of high-intensity pulses in thin plastic films but still has to be experimentally demonstrated.

The most straightforward strategy to reach all three key requirements at the same time is to employ OPCPA using thin nonlinear crystals and short pump pulses of less than 1 ps duration. First, a system based on this approach is capable to provide octave-spanning pulse spectra with less than two-cycle transform-limited pulse duration due to the large amplification bandwidth of the optical parametric amplification (OPA) technique. Second, the short pump pulse duration ensures an excellent amplified pulse contrast outside the 1 ps time window of the pump pulse. And third, the available aperture of lithium triborate (LBO) and potassium dideuterium phosphate (DKDP) crystals supports PW peak power as already demonstrated in multi-cycle (30–40 fs pulse duration) OPCPA laser systems [8,9].

The petawatt field synthesizer (PFS) [19], which is under development at Max-Planck Institute of Quantum Optics represents such a ps-pumped OPCPA system and exploits all advantages discussed above. The performance of the first two OPCPA stages of the PFS is presented in this paper.

The general scheme of the PFS system is shown in Fig. 1: the pump chain and the Ti:Sapphire amplifier are seeded by a common Ti:Sapphire master oscillator to ensure temporal synchronization of pump and signal pulses in the OPCPA stages [19–21]. The registered relative RMS timing jitter between pump and seed pulses is ~80 fs and currently limited mainly by mechanical vibrations in the system. Starting from the pump compressor, all parts of the system including the OPCPA chain and the experimental setup are located in vacuum (10^{-6} mbar) to prevent a beam quality degradation due to nonlinear distortions. In particular, the compressed pump pulses with an intensity of 100 GW/cm^2 would otherwise suffer from a B-integral of about 7 after propagation over 10 m in air. In the following sections, the different parts of the system will be discussed in detail.

2. SUB-PICOSECOND PUMP CHAIN

The current PFS pump chain is comprehensively described in [22–24] and will only be briefly summarized here. It is based on the chirped pulse amplification (CPA) technique and consists of a series of diode-pumped amplifiers featuring ytterbium-doped gain media. Starting with the 1030 nm output of a commercial Ti:Sa oscillator, the pulses are pre-amplified from the few-picojoule (pJ) to few-nanojoule (nJ) level in a Yb:glass fiber amplifier. The continuous amplified spontaneous emission (ASE) background generated in the fiber amplifier is mostly suppressed by a pulse picker based on a fast Pockels cell with ~150 ps gate width. Afterwards, the pulses are stretched by a Martinez-type stretcher to about 3 ns. An acousto-optic programmable dispersive filter (AOPDF, "Dazzler", FastLite) is used for spectral amplitude and phase shaping to counteract gain narrowing in the following amplifier stages and to control higher-order dispersion for optimal compression of the amplified pulses. Subsequently, the pulse energy is boosted by an Yb:glass regenerative amplifier and two Yb:YAG multi-pass amplifiers to 0.8 J. Compression in a folded Treacy-type compressor yields a pulse duration of 0.8 ps at an energy of 0.6 J. After spatial filtering and frequency doubling, 300 mJ pulses at 515 nm central wavelength are provided for the OPA stages (~2% losses in the spatial filter, ~55% second harmonic generation (SHG) efficiency, 1% rms energy fluctuations). About 4% of the available energy is used to pump the first OPA stage and the rest of the energy for the second stage.

3. CHOICE OF NONLINEAR CRYSTALS FOR OPCPA

The choice of nonlinear crystals is a crucial aspect for the design and construction of a high-power OPCPA [19,25]. One of the main criteria is the availability of crystals with large apertures of the order of 100 mm to provide amplified signal pulse energies in the Joule range while keeping pump intensities below the crystal damage threshold. Nowadays, state-of-the-art crystal growing technology provides such apertures for two types of nonlinear crystals: LBO and DKDP.

The main parameters of these crystals are presented in Table 1. As one can see, LBO is superior to DKDP in practically every aspect. Most important, it exhibits a higher effective second-order nonlinearity, which allows us to use thinner crystals at an identical OPA gain. This in turn makes the amplification more robust in the presence of wavefront aberrations (larger acceptance angle) and results in a broader gain bandwidth (smaller total phase mismatch) and a reduced impact of nonlinear distortions (smaller B-integral). Furthermore, we measured a more than twice higher damage threshold for anti-reflection-coated LBO compared to DKDP using our frequency-doubled PFS pump pulses at 515 nm. Another disadvantage of DKDP for our application is its limited spectral transmission at wavelengths longer than ~1500 nm even in highly deuterated DKDP: as the parametric amplification of signal components at 700–800 nm generates idler wavelengths in the range of 1450–1950 nm, linear absorption of these wavelengths reduces the overall OPA efficiency and, in systems with high average power, causes thermal issues such as a change of phase-matching conditions, thermal aberrations (including lensing), or damage. Finally, the significantly lower hygroscopy of LBO makes it easier to handle. The only notable advantage of DKDP is the larger maximum available aperture but continuous

Table 1. Parameters of LBO and DKDP Crystals

	LBO	DKDP
Effective $\chi^{(2)}$ nonlinearity	~0.82 pm/V [26]	~0.23 pm/V [26]
Transmission window (at 0.5 cm^{-1})	170–2300 nm [27]	200–1500 nm [28] (depends on the deuteration level)
Damage threshold (own measurement, $\tau \sim 0.8$ ps)	$4.3 \pm 0.8\,J/cm^2$ @ 1030 nm $1.0 \pm 0.2\,J/cm^2$ @ 515 nm (with AR coating)	$2.3 \pm 0.4\,J/cm^2$ @ 1030 nm $0.5 \pm 0.1\,J/cm^2$ @ 515 nm (with AR coating)
Hygroscopic susceptibility	very low	high
Maximum available aperture	~100 mm	~400 mm

progress in crystal growing technology over the past years now allows the production of 100 mm diameter LBO crystals [9], sufficient for light sources with PW-scale peak power. Overall, considering the advantages discussed above, LBO was chosen as crystal material for the PFS OPA stages.

4. PULSE FRONT MATCHING

To accomplish broadband phase matching, the OPA stages are set up in a non-collinear geometry where pump and signal beams intersect at an angle α_{int} inside the OPA crystals. For the design parameters of PFS (515 nm pump, 700–1400 nm seed, LBO type I) the optimal angle of intersection is $\alpha_{int} = 1.1°$. Due to the large beam diameters and the short pulse durations, this angle between the pulse fronts results in a substantially shrunk volume of spatio-temporal overlap as shown schematically in Fig. 2(a).

The importance of this effect can be estimated by considering the delay Δt between the pulse edges in the non-collinear plane. Taking into account the effective refractive index of LBO ($n_{eff.,515\,nm} \approx 1.6$), this delay is $\Delta t \approx 50\ fs/mm \times D$, where D is the beam diameter. At the second OPA stage for instance, the beam size is $D = 15$ mm, and hence a maximum delay of 0.75 ps is created. Since this delay is comparable to the pump pulse duration $\tau \sim 0.8$ ps, signal and pump pulses do only partially overlap, which in the OPA process results in a poor extraction of pump energy at the edges. Thus, the amplified signal beam profile becomes elliptical as shown in Fig. 4(a), and the OPA efficiency significantly decreases.

A solution to this issue is to tilt the pulse front of the pump as shown in Fig. 2(b) by an angle β to increase the overlap volume. Ideally, pump and signal pulse fronts are matched entirely by setting $\beta = \alpha_{int}$, which effectively reduces the mismatch angle $\gamma = \alpha_{int} - \beta$ to zero.

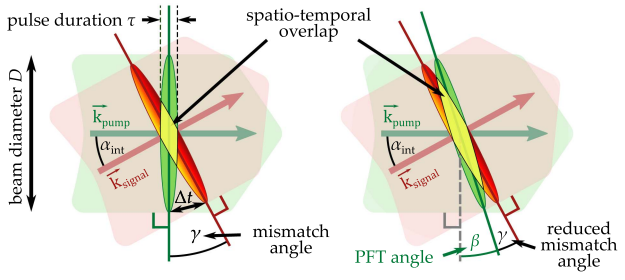

(a) non-matched pulse fronts (b) partially matched pulse fronts

Fig. 2. Spatio-temporal overlap of short pump and signal pulses in a non-collinear OPA stage. (a) Without further action, there is only a partial overlap. (b) By tilting the pulse front of the pump pulse, the overlap can be improved.

There exist several approaches to introduce a pulse front tilt (PFT), which are typically based on introducing angular dispersion in the beam [29,30]. Two viable methods for PFS are: (i) sending the pump beam through a pair of transmission gratings with a small intermediate angle or (ii) deliberately misaligning the reflection gratings of the pump compressor. Both options are applicable under appropriate experimental conditions. Option (i) has a number of issues, namely the limited available size of transmission gratings, their low damage threshold, and potential nonlinear distortions in the substrates; thus it can be used only for a low-energy beam (in our case, the pump for the first OPA stage). In contrast, option (ii) represents a cost-effective and efficient approach, as no additional optical elements are required and hence no losses or other detrimental effects need to be considered. This method is therefore preferred for the high-energy pump beam of the second stage.

The PFS pump compressor is built in folded geometry (for a schematic view of such a setup see, for example, [31]) and consists of a horizontal roof mirror (HRM), a vertical roof mirror (VRM), and a single dielectric grating with 1740 l/mm line density and an effective grating separation of ~6 m. Due to the folded design, the parallelism of the gratings is in practice controlled by adjusting the HRM, i.e., by setting its roof angle to a value different than the nominal 90°. The required PFT angle β_{cmp} at the compressor exit can be determined by taking into account the magnification $M \approx 0.8$ of the imaging telescopes between the compressor and second OPA stage,

$$\beta_{cmp} = M n_{eff.,\,515\,nm}\ \alpha_{int} \approx 1.4°. \tag{1}$$

It should be noted at this point that the PFT is directly transferred from the fundamental to the frequency-doubled pulses in the SHG process, and hence Eq. (1) equally applies to both beams. A small deviation of the PFT angle from the specified target value is acceptable and can be estimated via OPA simulations to be $\Delta\beta_{cmp} \approx 0.11°$, i.e., roughly 10% (for the specified beam size and noncollinear angle).

To experimentally realize the desired PFT angle β_{cmp} at the compressor exit, the angle of the HRM has to be set to $90° - \varepsilon$, where ε is calculated by adapting Eq. (7) in Pretzler *et al.* [29],

$$\varepsilon \approx \frac{1}{4}\frac{\cos\theta_{in}}{\tan\theta_{out}}\frac{d}{\lambda_0}(\beta_{cmp} \pm \Delta\beta_{cmp}) \approx 140 \pm 12\ \text{arcsec}. \tag{2}$$

Here, $\theta_{in} = 60°$ and $\theta_{out} = 67.8°$ are the angles of the incident and diffracted beams relative to the grating normal, $d = 1740\,l/mm$ is the grating line density, and $\lambda_0 = 1030$ nm is the central wavelength. As one can see from the equation, the

PFT tolerance $\Delta\beta_{cmp}$ defines the required alignment precision for the HRM. Experimentally, we were able to fulfill this requirement at about 3 arcsec alignment precision (corresponding to ~2 arcmin PFT) owing to the large lever (160 mm) and the motorization of the HRM mount.

To compensate for the modified optical path due to the ε-tilt of the HRM, the VRM has to be rotated accordingly, and the grating separation has to be readjusted by ~4 cm to yield again a compressed pulse. The remaining higher-order-dispersion terms after this compensation result in a negligible pulse elongation by less than 1% due to the relatively narrow pump bandwidth of ~3 nm.

As mentioned before, the PFT is created by introducing an angular chirp, which raises the question of whether this could result in negative side effects. In the described scheme, the angular chirp is about 24 μrad/nm, which yields an angle spread of ~75 μrad for the full bandwidth of about 3 nm in the fundamental beam. Compared to the independently measured acceptance angle of the SHG crystal (DKDP, type II, 6 mm) of ~8.7 mrad (full width at half-maximum, FWHM), this spread is small, and accordingly no adverse effect on the SHG efficiency was found. Furthermore, the imaging system from the compressor output to the SHG crystal and then to the OPA crystal guarantees at these points the absence of any spatial chirp that would otherwise be caused by free-space propagation of the angularly chirped beam.

In conclusion, no drawback was found in the suggested scheme of pulse front matching by compressor "misalignment." One more modification to the PFS system, however, became necessary: since the pump pulses for the first and second OPCPA stage are derived from the same frequency-doubled pulse with a beam splitter, but afterwards pass different telescopes on the way to the respective OPCPA stages, the PFT introduced in the compressor matches the pulse fronts at the second stage but results in a significant mismatch at the first stage. To compensate for this effect, a pair of transmission gratings (Fraunhofer IOF, 2000 lines/mm, Littrow angle 31°, relative angle ~1°) was installed in the pump beam path for the first OPCPA stage directly behind the beam splitter. As the intensity at this location is low, the prior mentioned damage threshold and B-integral issues of transmission gratings are uncritical for this solution. Furthermore, the placement of the gratings close to the telescope's image plane at the SHG crystal ensures that the emerging spatial chirp is nearly compensated at the OPCPA stage.

5. BROADBAND SEED GENERATION

Based on the phase matching properties of LBO crystals used in the OPA stages of PFS and the pump wavelength of 515 nm, seed pulses in the spectral range of 700–1400 nm are required. Accessing this range with multi-μJ pulse energy while maintaining a high spatial and temporal quality of the pulses is a non-trivial task.

The currently implemented seed generation scheme consists of two main parts as shown in Fig. 3(a): in a first step, the output from a commercial Ti:Sapphire amplifier (Femtopower CompactPro) is spectrally broadened in two cascaded hollow-core fibers (HCFs) filled with neon gas. This scheme has already been described in [32]. In a second step, the resulting broadband pulses are temporally cleaned by cross-polarized wave (XPW) generation, a third-order nonlinear process described, e.g., in [33]. This second step becomes necessary due to strong modulations in the spectral amplitude and phase of the generated pulses, which originate from the nonlinear broadening process in the HCFs. As these

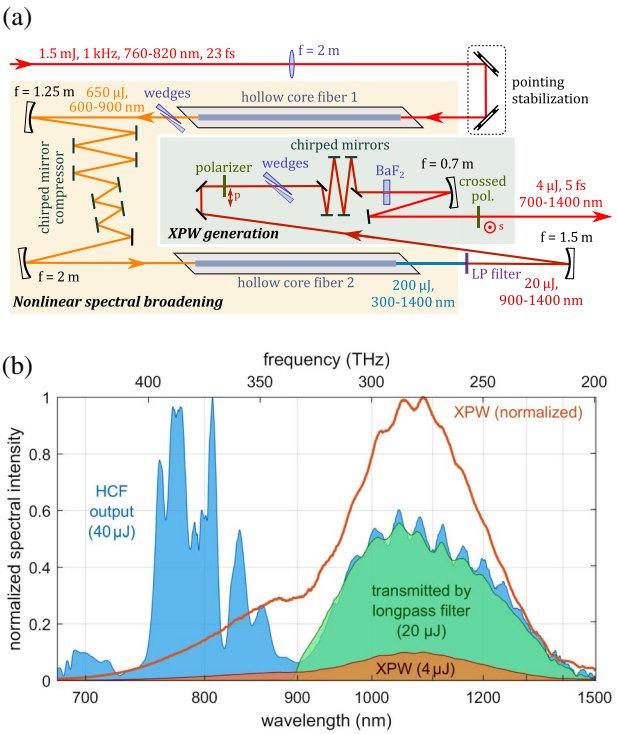

Fig. 3. Broadband seed generation: (a) schematic setup with spectral broadening in two consecutive HCFs and temporal cleaning via XPW generation. (b) Measured spectra: blue is the spectrum after the second HCF (only wavelengths >680 nm displayed), green is the transmission through the installed longpass filter, and red is the (scaled or normalized) XPW spectrum after the crossed polarizer, i.e., the final seed for OPCPA.

modulations were found to get enhanced in the OPCPA process (especially in saturation) and prevent temporal compression of the amplified pulses, they have to be removed. To this end, the output of the second HCF is filtered with a dielectric longpass filter (LP900, Asahi Spectra, $\lambda_{cut} = 900$ nm) and is imaged with a spherical mirror ($f = 1500$ mm) onto a BaF_2 crystal (1 mm, z-cut) that serves as the $\chi^{(3)}$-medium for the XPW generation process. In between, a polarizer (Thorlabs, LPVIS) selects the p-polarization from the slightly elliptically polarized output of the HCF. A pair of fused silica wedges and four chirped mirrors (PC503, UltraFast Innovations) are used for temporal compression. A second polarizer with crossed orientation relative to the first one selects the s-polarized XPW. After the BaF_2 crystal, the beam is collimated for transport to the OPCPA stages.

The installed longpass filter serves multiple purposes: first, it protects the subsequent silver mirrors against ultraviolet radiation from the broadband pulses after the HCFs. Second, it shifts the central wavelength of the filtered pulses to about 1050 nm and therefore supports spectral broadening in the range of interest (700–1400 nm) by XPW generation and by other $\chi^{(3)}$-effects (such as self-phase modulation), which are triggered simultaneously due to the high intensities (~15 TW/cm^2) at the crystal. And finally, it removes weak but temporally long artifacts at wavelengths below 900 nm that we found are otherwise able to leak through the crossed polarizers.

The measured XPW generation efficiency of 20% is comparatively high, considering the theoretical limit for Gaussian pulses of 28% [33]. The spectra of the broadband pulses before and after

the process are shown in Fig. 3(b) (note that spectral components below 680 nm, which contain a large fraction of the total HCF output pulse energy, are not displayed). As one can see, the cross-polarized pulses feature a very smooth spectrum that fully covers the designed spectral range of 700–1400 nm.

6. PARAMETRIC AMPLIFICATION

The currently implemented part of the PFS system consists of two OPCPA stages with LBO crystals (type I, $\theta = 90°$, $\varphi = 14.5°$) of 4 mm thickness at the first stage and 2 mm at the second stage. The seed pulses are stretched to ~600 fs before the first OPCPA stage by propagation through 12 m of air (optical path from seed generation setup to OPCPA) and several millimeters of CaF_2 and fused silica substrates (polarizer, vacuum window, and wedges/subtrates for dispersion control). To suppress air turbulences that could otherwise affect pointing and timing jitter, most of the optical path is covered. Sizes of both pump and seed beams are 3 mm at the first stage and 15 mm at the second stage. The pump intensity is about 100 GW/cm^2 at both stages.

Figure 4 displays the amplified signal beam profile after the second OPCPA stage for two different pulse front tilt settings of the pump pulses. In Fig. 4(a) the effect of elliptical cropping can be seen that occurs when choosing a tilt angle different to the non-collinear angle between signal and pump beam, thus resulting in poor pulse overlap. In contrast, Fig. 4(b) shows the case of properly matched pulse fronts where only the imprint of beam profile distortions of the pump beam are visible.

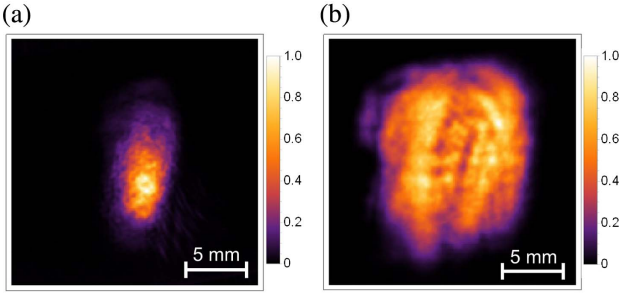

Fig. 4. Amplified signal beam profile after the second OPCPA stage in the case of (a) non-matched pulse fronts, (b) matched pulse fronts.

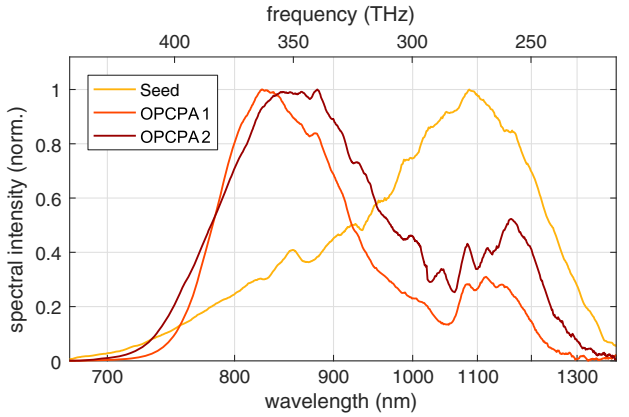

Fig. 5. Input spectrum and parametrically amplified spectra after the first and the second OPCPA stage.

In the case of matched pulse fronts, amplified pulse energies of 1.3 mJ after the first and 46 mJ after the second OPCPA stage were achieved. The respective spectra are shown in Fig. 5 and feature two broad maxima at 850 nm and 1150 nm with a decline around 1000 nm. This spectral shape is determined by the phase-matching properties of LBO under the specified experimental conditions. The corresponding gain narrowing is partially counteracted by the spectral shape of the seed to support a broader amplified spectrum. The final spectrum after both stages supports a transform-limited pulse duration of 5.1 fs at 900 nm central wavelength corresponding to less than two optical cycles of the electric field. Substantial effort was made to compress the amplified pulses close to this limit, which will be described in the following.

7. TEMPORAL COMPRESSION

Good compression of parametrically amplified broadband pulses requires not only perfect matching of dispersion in the stretcher, compressor, and other parts of the system, but also a compensation of the so-called optical parametric phase (OPP) [34,35]. This phase is accumulated in the OPA process due to the phase mismatch between the interacting waves and manifests itself as an additional spectral phase $\varphi_{OPA}(\omega)$. Performing a simple estimation of the OPP by adapting Eq. (11) in [34] to our experimental conditions and calculating the corresponding group delay (GD) $GD_{OPA} = \partial\varphi_{OPA}/\partial\omega$ yields a GD spread of about 60 fs over the bandwidth of 700–1200 nm (cf. Fig. 6). To check this theoretical prediction, we measured the OPP by spectral interferometry between a part of the signal beam split off before and bypassing the OPA stages (first arm) and the pulses passing through the OPA stages (second arm). The difference between the phases for amplified and unamplified (pump beam blocked) signal pulses yields the OPP. The experimentally determined values are shown in Fig. 6 and are in good agreement with the simulated curves.

When comparing the 60 fs GD spread with the target pulse duration of a few femtoseconds, it is obvious that for a successful compression the OPP has to be taken into account in the dispersion management. This is even more important, as the OPP contains higher-order dispersion terms that cannot be compensated by simple means, for instance by a pair of wedges.

The measured OPP was thus included in the dispersion design for the chirped mirror compressor (CMC) that re-compresses the positively chirped signal pulses after amplification. It is set up in vacuum and consists of twelve negatively chirped mirrors produced in-house. To allow for a certain degree of flexibility,

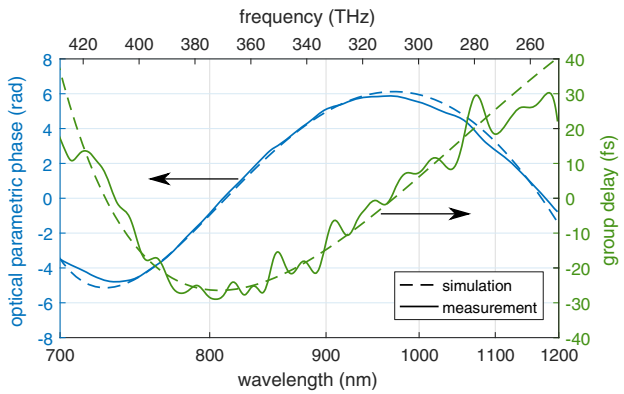

Fig. 6. Simulated and measured optical parametric phase.

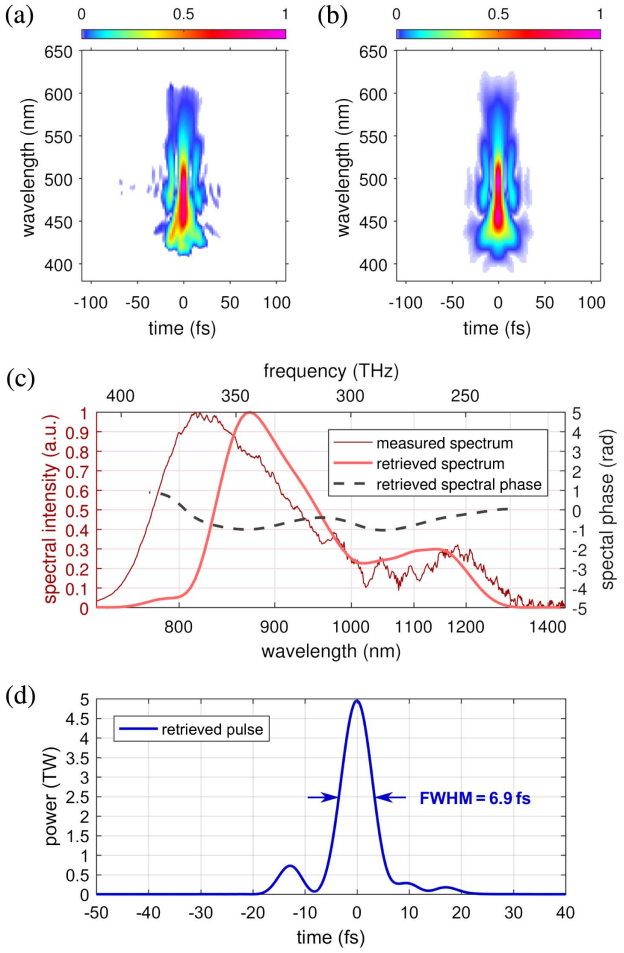

Fig. 7. Temporal compression of parametrically amplified pulses. (a) Measured and (b) retrieved SHG-FROG traces. (c) Measured and retrieved spectra. (d) Retrieved temporal pulse shape.

two types of mirrors with different higher-order dispersions were coated and implemented. For damage threshold reasons, mirror substrates with two inch diameter were used. The compressed pulse duration was determined and optimized with the SHG-frequency-resolved optical gating (FROG) technique in a home-built single-shot setup (similar to [36]) using a beta-barium borate (BBO) crystal with about 5 μm thickness. The measured and retrieved traces are shown in Figs. 7(a) and 7(b), respectively, and correspond to the temporal shape displayed in Fig. 7(d). The difference between the spectrum measured with a spectrometer and the retrieved one [Fig. 7(c)] is due to phase matching and transmission limitations of the FROG setup. While not entirely compressed, the pulses exhibit a duration of 6.9 ± 0.8 fs (sub-2.5 cycle at 900 nm central wavelength).

The measured transmission of the CMC is 91%, which corresponds to 42 mJ output energy and yields a peak power of 5 TW, taking into account the retrieved temporal shape. To further improve the compression towards the Fourier-limited pulse duration below 6 fs, the implementation of a spatial light modulator is in preparation (more details in Section 11).

8. TEMPORAL CONTRAST

To determine the temporal contrast of the amplified pulses, a third-order autocorrelation trace was measured (Tundra, UltraFast

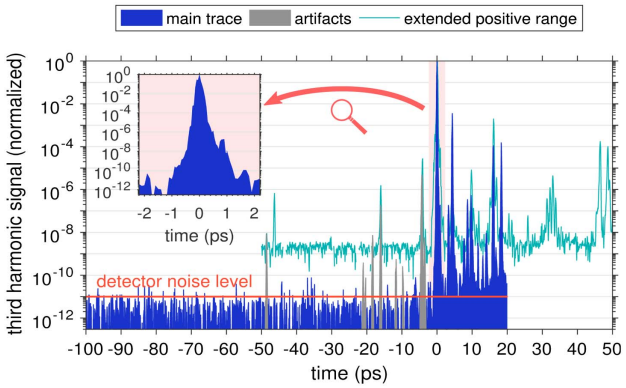

Fig. 8. Temporal contrast as measured by third-order autocorrelation. Pre-pulse features marked in gray are presumably measurement artifacts created by post-pulses. The light blue line shows a more symmetric AC trace in time, measured with a different AC setup with less dynamic range. It demonstrates that the apparent −48 ps pre-pulse is an artifact of the 48 ps post-pulse. The total number of pre-/post-pulses is different due to different internal reflections in the two AC setups.

Innovations), which is shown in Fig. 8. Due to bandwidth limitations of the device, only the wavelength range of approximately 780–820 nm contributes to the measured signal. As this range, however, corresponds to the spectral band of the Ti:Sapphire amplifier that drives the generation of the broadband signal pulses, it covers the spectral region with presumably the worst contrast. In this wavelength range, a contrast ratio of more than 10^{11} is demonstrated, reaching the noise level of the detector. Since the temporal resolution of the autocorrelator (AC) is about 100 fs FWHM, this ratio probably even underestimates the peak intensity and contrast of the real pulse ($\tau \sim 7$ fs) by an order of magnitude.

While the plot shows several peaks before the main pulse, we can consider them as measurement artifacts originating from post-pulses, which in turn are created by double reflections in vacuum windows, OPA crystals, and substrates used for dispersion control. This assumption is justified due to the symmetric positions of the pulses around the main peak and their relative power-scaling (the amplitude of a pre-pulse-like measurement artifact is equal to the square of the amplitude of the corresponding post-pulse). Furthermore, when removing substrates for dispersion control in a later measurement, the simultaneous vanishing of the corresponding pre- and post-pulses around ±20 ps was observed. Note that, unfortunately, the scanning range of our main autocorrelator is limited in the positive direction by 20 ps in order to have a longer range in the negative direction where pre-pulses would be located. This is the reason why we additionally present the trace with extended positive range measured with another AC setup having worse dynamical range and introducing a couple of extra peaks coming from double reflection of the internal optical components.

When zooming into the measured contrast curve (inset in Fig. 8), the absence of any temporal pedestal is evident with the intensity dropping to the noise level of the detector at approximately 1 ps before the main pulse. This remarkable property is a consequence of the short pump pulse duration of the PFS and—to the best of our knowledge—makes the system unique among existing light sources with more than 1 TW peak power.

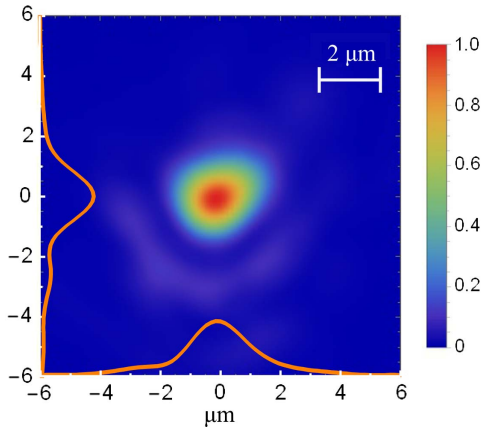

Fig. 9. Measured intensity distribution of the amplified pulses in the focal plane of an f/1.6, 90° off-axis parabolic mirror. The orange lines show the integrated distribution along the x and y directions.

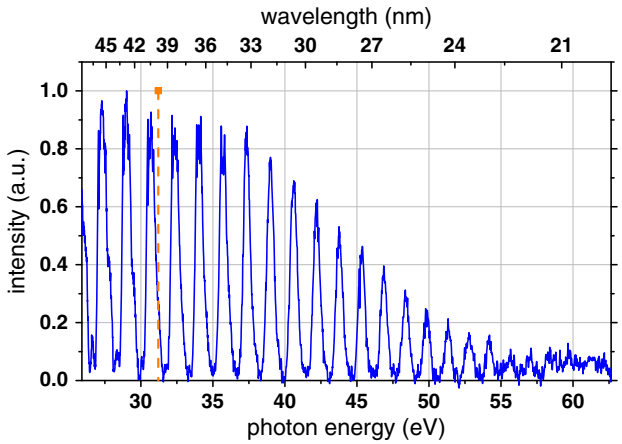

Fig. 10. Typical high-harmonic spectrum measured at ~15 mJ pulse energy on target. The dashed line marks the spectral cutoff for coherent wake emission thus proving the generation of ROM harmonics.

9. FOCUSABILITY

For experiments in high-field physics, maximizing the peak intensity is of great importance. Therefore, the amplified pulses were focused in the experimental chamber with an f/1.6, 90° off-axis parabolic mirror onto the target. The energy distribution in focus was measured by imaging the attenuated beam onto a charge-coupled device (CCD) camera (detection range ~350–1100 nm). For this purpose, an achromatic infinity-corrected microscope objective (40 × /0.65) and an achromatic lens with 200 mm focal length were used. The measured beam profile in the focal plane is shown in Fig. 9 and corresponds to a relativistic intensity of $6.9 \pm 1.9 \times 10^{19}$ W/cm^2 ($a_0 \sim 6.1$), taking into account the beamline transmission of 92% from the CMC exit to the target. The specified uncertainty is mainly determined by the uncertainty in pulse duration and the fact that ~20% of the pulse energy is located in the spectral range above 1100 nm, which is not detectable by the focus diagnostic CCD.

10. FIRST EXPERIMENTAL RESULTS ON SURFACE HIGH-HARMONIC GENERATION

One of the most interesting and promising applications for the PFS system is the generation of attosecond pulses in the relativistic intensity regime based on the relativistic oscillating mirror (ROM) effect which—according to theoretical predictions—should provide a considerable increase of the conversion efficiency compared to gas harmonics [2]. The PFS is expected to be an ideal tool to perform such an experiment, since the ROM high-harmonic generation (HHG) process demands a high pulse contrast [37], and the generation of isolated attosecond pulses additionally requires a few-cycle pulse duration [2]. A desirable feature that our system is lacking in its current state is a stabilized CEP of the output pulses. However, by tagging the CEP with single-shot diagnostics such as a stereo-above threshold ionization (ATI) phase meter or an f–2f interferometer, all shots can be sorted according to their CEP values [4,38]. In the CEP-stabilized case, the CEP is scanned, while in the CEP-unstabilized case, it is tagged and the data is sorted, so the number of shots and acquisition time is comparable for the both cases. Therefore, the absence of CEP stability is not a drawback for experiments aiming at the investigation of the CEP dependence of a phenomenon; for example, for the measurement of the dependence of the HHG spectrum on the CEP of the driving pulses. However, many applications, for example XUV-pump/XUV-probe spectroscopy, require a stable CEP optimized for the generation of isolated attosecond pulses. Therefore, we plan to stabilize the CEP of the amplified pulses in the coming upgrade.

We prepared an experimental ROM HHG setup in the following configuration: the amplified and compressed pulses are focused on the target with an off-axis parabolic mirror as already described before. The angle of incidence onto the target is about 45° with a p-polarized input beam. The target is a fused silica substrate fixed in a motorized rotation mount to provide a fresh target spot for each shot. The rotation mount is additionally installed on a linear x–y stage to longitudinally place the target surface in the laser focus and to enable a parallel shift of the target to start a fresh ring of target spots.

The radiation reflected by the plasma mirror contains both the fundamental beam and harmonics. The fundamental radiation, being orders of magnitude more intense than its harmonics, is filtered out by a 200 nm thick aluminum filter. The transmitted harmonic radiation is detected with a home-built flat-field spectrometer consisting of a gold-coated grazing incidence aberration-corrected concave grating (Hitachi Part No. 001-0266) and an XUV CCD camera. At the time of the experimental campaign, only ~15 mJ compressed pulse energy was available on target. Typical harmonic spectra achieved with these pulses are shown in Fig. 10 where ROM harmonics with photon energies exceeding 55 eV are visible. These preliminary but quite promising results can be considered as an ultimate test of the performance of PFS. As further optimization of the system is ongoing, we expect to see an improvement of the harmonics performance and more detailed data in the near future. These results will be published separately.

11. UPGRADE PLANS

The setup and performance presented in the previous sections provide a major milestone towards the ultimate goal of the PFS project to reach PW-scale peak power with few-cycle light pulses. Currently, an upgrade of the described system is under way that is expected to boost the output power by more than an order of magnitude into the 100 TW regime. It includes

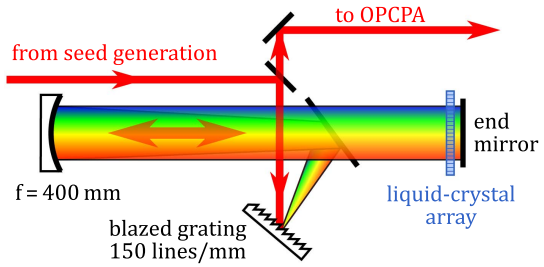

Fig. 11. Scheme of an adaptive optical pulse shaper to control the dispersion of the broadband signal pulses before amplification.

an additional Yb:YAG pump amplifier with more than 10 J output energy at the same pulse duration (~800 fs) and repetition rate (10 Hz) as before. At the same time, the OPCPA setup will be extended with a third and fourth stage, which are both pumped by the second harmonic of the new pump amplifier (pump recycling) and consist of large-diameter (80 mm) LBO crystals. At 3–4 times larger beam sizes, matching the pulse fronts in these stages is even more important than for the stages before. To do so, the same approach will be used as explained for the second OPCPA stage in Section 4, i.e., by adjustment of the pump compressor. Due to the separate beam paths in the compressor, an independent optimization of the PFT for the second and third/fourth OPCPA stage is possible.

For an improved compression of the amplified broadband pulses we are preparing an optical pulse shaper to compensate for higher-order dispersion terms—especially those introduced by the OPP, which depend on phase matching and gain and may be subject to changes from day to day. The setup is schematically shown in Fig. 11 and consists of a blazed grating placed in the image plane of a $4f$ system and a one-dimensional liquid-crystal spatial light modulator (SLM-S640, Jenoptik) located in the Fourier plane of the system. Due to the spatial chirp, a wavelength-dependent phase shift of up to $\sim 4\pi$ can be introduced by modifying the optical path length in each pixel of the SLM.

A potential drawback of the scheme, besides the loss of seed energy (~60% transmission), is the degradation of the temporal contrast due to the pixelation of the SLM. In an experimental test with unamplified pulses, however, we could show that no temporal features stronger than 10^{-5} relative to the main peak (detection limit of the measurement) are created. This is in agreement with a theoretical analysis that predicts a degradation on the order of 10^{-7} and furthermore shows that the generated artifacts are located in time well outside the pump window of ± 1 ps. Therefore, as the shaper will be placed in the signal beam path before the OPCPA stages, these artifacts would not be amplified, and hence no noticeable contrast degradation of the final pulses is expected. As mentioned before, the broadband seed pulses and therefore also the parametrically amplified pulses are currently not CEP stabilized, which requires CEP tagging for experimental applications. Hence, in the upgrade process it is planned to implement an alternative seed generation scheme to achieve passive CEP stability.

12. CONCLUSION

In summary, we reported on the performance of the first two OPCPA stages of the PFS system that deliver sub-7 fs near-infrared pulses at 10 Hz repetition rate with 5 TW peak power and an excellent contrast of better than 10^{11}, which is maintained until ~1 ps before the main pulse. By focusing the beam with an off-axis parabolic mirror, relativistic intensities of about $6.9 \pm 1.9 \times 10^{19}$ W/cm^2 were achieved on target. The usability of the generated pulses was demonstrated in an experiment by generating high harmonics from a solid surface. A planned system upgrade is expected to boost the peak power by more than an order of magnitude towards 100 TW. Furthermore, we aim to improve the temporal compression of the amplified pulses with an adaptive shaper to achieve a pulse duration below 6 fs. At these target parameters, the system will be a unique and powerful tool for experiments in relativistic attosecond science.

Funding. Horizon 2020 Framework Programme (H2020) (633053 within the framework of the EUROfusion); Deutsche Forschungsgemeinschaft (DFG) (EXC 158, TR-18); Max-Planck-Gesellschaft (MPG) (IMPRS-APS, PFS-grant).

Acknowledgment. The authors greatly acknowledge the contributions made by the former members of the PFS team, namely, Christoph Skrobol, Christoph Wandt, Sandro Klingebiel, and Izhar Ahmad. Furthermore, we thank George Tsakiris for many useful discussions about the surface harmonics experiment and Alexander Weigel from UltraFast Innovations GmbH for his help with the temporal contrast measurement. We would like to acknowledge the support of Dmitrii Kormin and Laszlo Veisz who helped us with the preparation of the SHHG experiments.

REFERENCES

1. G. Mourou, T. Tajima, and S. V. Bulanov, "Optics in the relativistic regime," Rev. Mod. Phys. **78**, 309–371 (2006).
2. G. D. Tsakiris, K. Eidmann, J. Meyer-ter-Vehn, and F. Krausz, "Route to intense single attosecond pulses," New J. Phys. **8**, 19 (2006).
3. F. Krausz and M. Ivanov, "Attosecond physics," Rev. Mod. Phys. **81**, 163–234 (2009).
4. T. Wittmann, B. Horvath, W. Helml, M. G. Schätzel, X. Gu, A. L. Cavalieri, G. G. Paulus, and R. Kienberger, "Single-shot carrier-envelope phase measurement of few-cycle laser pulses," Nat. Phys. **5**, 357–362 (2009).
5. B. Dromey, S. Kar, M. Zepf, and P. Foster, "The plasma mirror—a subpicosecond optical switch for ultrahigh power lasers," Rev. Sci. Instrum. **75**, 645–649 (2004).
6. V. Yanovsky, V. Chvykov, G. Kalinchenko, P. Rousseau, T. Planchon, T. Matsuoka, A. Maksimchuk, J. Nees, G. Cheriaux, G. Mourou, and K. Krushelnick, "Ultra-high intensity 300 TW laser at 0.1 Hz repetition rate," Opt. Express **16**, 2109 (2008).
7. Y. Chu, Z. Gan, X. Liang, L. Yu, X. Lu, C. Wang, X. Wang, L. Xu, H. Lu, D. Yin, Y. Leng, R. Li, and Z. Xu, "High-energy large-aperture Ti:sapphire amplifier for 5 PW laser pulses," Opt. Lett. **40**, 5011–5014 (2015).
8. V. V. Lozhkarev, G. I. Freidman, V. N. Ginzburg, E. V. Katin, E. A. Khazanov, A. V. Kirsanov, G. A. Luchinin, A. N. Mal'shakov, M. A. Martyanov, O. V. Palashov, A. K. Poteomkin, A. M. Sergeev, A. A. Shaykin, and I. V. Yakovlev, "Compact 0.56 Petawatt laser system based on optical parametric chirped pulse amplification in KD*P crystals," Laser Phys. Lett. **4**, 421–427 (2007).
9. L. Yu, X. Liang, L. Xu, W. Li, C. Peng, Z. Hu, C. Wang, X. Lu, Y. Chu, Z. Gan, X. Liu, Y. Liu, X. Wang, H. Lu, D. Yin, Y. Leng, R. Li, and Z. Xu, "Optimization for high-energy and high-efficiency broadband optical parametric chirped-pulse amplification in LBO near 800 nm," Opt. Lett. **40**, 3412–3415 (2015).
10. D. Herrmann, L. Veisz, R. Tautz, F. Tavella, K. Schmid, V. Pervak, and F. Krausz, "Generation of sub-three-cycle, 16 TW light pulses by using noncollinear optical parametric chirped-pulse amplification," Opt. Lett. **34**, 2459–2461 (2009).
11. E. W. Gaul, M. Martinez, J. Blakeney, A. Jochmann, M. Ringuette, D. Hammond, T. Borger, R. Escamilla, S. Douglas, W. Henderson, G. Dyer, A. Erlandson, R. Cross, J. Caird, C. Ebbers, and T. Ditmire, "Demonstration of a 1.1 petawatt laser based on a hybrid optical

parametric chirped pulse amplification/mixed Nd:glass amplifier," Appl. Opt. **49**, 1676–1681 (2010).
12. Z. Wang, C. Liu, Z. Shen, Q. Zhang, H. Teng, and Z. Wei, "High-contrast 1.16 PW Ti:sapphire laser system combined with a doubled chirped-pulse amplification scheme and a femtosecond optical-parametric amplifier," Opt. Lett. **36**, 3194–3196 (2011).
13. A. Wirth, M. Th. Hassan, I. Grguraš, J. Gagnon, A. Moulet, T. T. Luu, S. Pabst, R. Santra, Z. A. Alahmed, A. M. Azzeer, V. S. Yakovlev, V. Pervak, F. Krausz, and E. Goulielmakis, "Synthesized light transients," Science **334**, 195–200 (2011).
14. S. Sartania, Z. Cheng, M. Lenzner, G. Tempea, Ch. Spielmann, F. Krausz, and K. Ferencz, "Generation of 0.1-TW 5-fs optical pulses at a 1-kHz repetition rate," Opt. Lett. **22**, 1562–1564 (1997).
15. D. E. Rivas, A. Borot, D. E. Cardenas, G. Marcus, X. Gu, D. Herrmann, J. Xu, J. Tan, D. Kormin, G. Ma, W. Dallari, G. D. Tsakiris, I. B. Földes, S.-W. Chou, M. Weidman, B. Bergues, T. Wittmann, H. Schröder, P. Tzallas, D. Charalambidis, O. Razskazovskaya, V. Pervak, F. Krausz, and L. Veisz, "Next generation driver for attosecond and laser-plasma physics," Sci. Rep. **7**, 5224 (2017).
16. R. Budriūnas, T. Stanislauskas, J. Adamonis, A. Aleknavičius, G. Veitas, D. Gadonas, S. Balickas, A. Michailovas, and A. Varanavičius, "53 W average power CEP-stabilized OPCPA system delivering 5.5 TW few cycle pulses at 1 kHz repetition rate," Opt. Express **25**, 5797–5806 (2017).
17. B. Gilicze, A. Barna, Z. Kovács, S. Szatmári, and I. B. Földes, "Plasma mirrors for short pulse KrF lasers," Rev. Sci. Instrum. **77**, 083109 (2006).
18. G. Mourou, S. Mironov, E. Khazanov, and A. Sergeev, "Single cycle thin film compressor opening the door to Zeptosecond-Exawatt physics," Eur. Phys. J. Spec. Top. **223**, 1181–1188 (2014).
19. Zs. Major, S. A. Trushin, I. Ahmad, M. Siebold, C. Wandt, S. Klingebiel, T.-J. Wang, J. A. Fülöp, A. Henig, S. Kruber, R. Weingartner, A. Popp, J. Osterhoff, R. Hörlein, J. Hein, V. Pervak, A. Apolonski, F. Krausz, and S. Karsch, "Basic concepts and current status of the Petawatt Field Synthesizer–a new approach to ultrahigh field generation," Rev. Laser Eng. **37**, 431–436 (2009).
20. C. Y. Teisset, N. Ishii, T. Fuji, T. Metzger, S. Köhler, R. Holzwarth, A. Baltuska, A. M. Zheltikov, and F. Krausz, "Soliton-based pump-seed synchronization for few-cycle OPCPA," Opt. Express **13**, 6550–6557 (2005).
21. S. Klingebiel, I. Ahmad, C. Wandt, C. Skrobol, S. A. Trushin, Z. Major, F. Krausz, and S. Karsch, "Experimental and theoretical investigation of timing jitter inside a stretcher-compressor setup," Opt. Express **20**, 3443–3455 (2012).
22. S. Klingebiel, C. Wandt, C. Skrobol, I. Ahmad, S. A. Trushin, Z. Major, F. Krausz, and S. Karsch, "High energy picosecond Yb:YAG CPA system at 10 Hz repetition rate for pumping optical parametric amplifiers," Opt. Express **19**, 5357–5363 (2011).
23. C. Wandt, S. Klingebiel, S. Keppler, M. Hornung, M. Loeser, M. Siebold, C. Skrobol, A. Kessel, S. A. Trushin, Z. Major, J. Hein, M. C. Kaluza, F. Krausz, and S. Karsch, "Development of a Joule-class Yb:YAG amplifier and its implementation in a CPA system generating 1 TW pulses," Laser Photon. Rev. **8**, 875–881 (2014).
24. M. Krüger, A. Münzer, V. E. Leshchenko, A. Kessel, O. Jahn, A. Schwarz, C. Skrobol, S. Klingebiel, C. Wandt, S. A. Trushin, F. Krausz, Z. Major, and S. Karsch, "Picosecond, Joule-Class Yb:YAG CPA amplifier for pumping a high contrast OPCPA system," in preparation.
25. C. Skrobol, I. Ahmad, S. Klingebiel, C. Wandt, S. A. Trushin, Zs. Major, F. Krausz, and S. Karsch, "Broadband amplification by picosecond OPCPA in DKDP pumped at 515 nm," Opt. Express **20**, 4619–4629 (2012).
26. D. A. Roberts, "Simplified characterization of uniaxial and biaxial nonlinear optical crystals: a plea for standardization of nomenclature and conventions," IEEE J. Quantum Electron. **28**, 2057–2074 (1992).
27. C. Chen, Y. Wu, A. Jiang, B. Wu, G. You, R. Li, and S. Lin, "New nonlinear-optical crystal: LiB3O5," J. Opt. Soc. Am. B **6**, 616–621 (1989).
28. A. Dyan, G. Duchateau, S. Eslava, J. L. Stehle, D. Damiani, and H. Piombini, "Transmission measurements in rapid growth KDP and DKDP crystals," J. Mod. Opt. **56**, 27–31 (2009).
29. G. Pretzler, A. Kasper, and K. J. Witte, "Angular chirp and tilted light pulses in CPA lasers," Appl. Phys. B **70**, 1–9 (2000).
30. J. A. Fülöp, Zs. Major, A. Henig, S. Kruber, R. Weingartner, T. Clausnitzer, E.-B. Kley, A. Tünnermann, V. Pervak, A. Apolonski, J. Osterhoff, R. Hörlein, F. Krausz, and S. Karsch, "Short-pulse optical parametric chirped-pulse amplification for the generation of high-power few-cycle pulses," New J. Phys. **9**, 438 (2007).
31. M. Lai, S. T. Lai, and C. Swinger, "Single-grating laser pulse stretcher and compressor," Appl. Opt. **33**, 6985–6987 (1994).
32. I. Ahmad, S. Trushin, Zs. Major, C. Wandt, S. Klingebiel, T.-J. Wang, V. Pervak, A. Popp, M. Siebold, F. Krausz, and S. Karsch, "Frontend light source for short-pulse pumped OPCPA system," Appl. Phys. B **97**, 529–536 (2009).
33. S. Kourtev, N. Minkovski, L. Canova, and A. Jullien, "Improved nonlinear cross-polarized wave generation in cubic crystals by optimization of the crystal orientation," J. Opt. Soc. Am. B **26**, 1269–1275 (2009).
34. I. N. Ross, P. Matousek, G. H. C. New, Geoffrey, and K. Osvay, "Analysis and optimization of optical parametric chirped pulse amplification," J. Opt. Soc. Am. B **19**, 2945–2956 (2002).
35. S. Demmler, J. Rothhardt, S. Hädrich, J. Bromage, J. Limpert, and A. Tünnermann, "Control of nonlinear spectral phase induced by ultrabroadband optical parametric amplification," Opt. Lett. **37**, 3933–3935 (2012).
36. S. Akturk, C. D'Amico, and A. Mysyrowicz, "Measuring ultrashort pulses in the single-cycle regime using frequency-resolved optical gating," J. Opt. Soc. Am. B **25**, A63–A69 (2008).
37. M. Behmke, D. Brügge, C. Rödel, M. Cerchez, D. Hemmers, M. Heyer, O. Jäckel, M. Kübel, G. G. Paulus, G. Pretzler, A. Pukhov, M. Toncian, T. Toncian, and O. Willi, "Controlling the spacing of attosecond pulse trains from relativistic surface plasmas," Phys. Rev. Lett. **106**, 185002 (2011).
38. X. Ren, A. M. Summers, K. Raju, A. Vajdi, V. Makhija, C. W. Fehrenbach, N. G. Kling, K. J. Betsch, Z. Wang, M. F. Kling, K. D. Carnes, I. Ben-Itzhak, C. Trallero-Herrero, and V. Kumarappan, "Single-shot carrier-envelope-phase tagging using an f-2f interferometer and a phase-meter: a comparison," J. Opt. **19**, 124017 (2017).

130.183.92.7 {ts '2018-04-30 09:08:29'}